21th International Conference on Renewable Energies and Power Quality (ICREPQ'23)
Madrid (Spain), 24th to 26th May 2023
Renewable Energy and Power Quality Journal (RE&PQJ)
ISSN 2172-038 X, Volume No.21, July 2023

Verification of the uninterrupted transition from grid parallel to island grid operation of the Virtual Synchronous Machine in a microgrid

Steven Reineke[1], Dirk Turschner[2], Ines Hauer[3] and Hans-Peter Beck[4]

[1234]Institute of Electrical Power Engineering and Energy Systems
Clausthal University of Technology
Leibnizstraße 28, 38678 Clausthal-Zellerfeld (Germany)
[1]Phone number: +49-5323-72-2929, e-mail: steven.reineke@tu-clausthal.de
[2]Phone number: +49-5323-72-2592, e-mail: dirk.tuschner@tu-clausthal.de
[3]Phone number: +49-5323-72-2299, e-mail: ines.hauer@tu-clausthal.de
[4]Phone number: +49-5323-72-2570, e-mail: hans-peter.beck@tu-clausthal.de

Abstract

The classic energy supply system is mainly based on the stabilising properties of electromechanical synchronous generators. The structural change of the electrical energy supply system towards a decentralised grid structure means that ancillary services must now also be provided at the distribution grid level. The Virtual Synchronous Machine (VISMA) was developed at the Institute of Electrical Power Engineering at the Clausthal University of Technology with the aim of making a decentralised generation unit in the grid behave like a real synchronous machine and thus actively provide relevant ancillary services. The VISMA is based on a three-phase inverter that can comply with grid requirements by adding an energy storage device in the DC link and using a special control algorithm.
The focus of the investigations shown here is on the uninterrupted transition from grid-parallel operation of the VISMA to island grid operation and the subsequent stable continued operation of this island grid. A controller changeover, as most feed-in inverters would require in order to change the operating mode, is not necessary here. It is shown that the transients have subsided after 5 ms, which means that the VISMA has completely taken over the supply of the load, and the new steady state is reached after 40 ms.

Keywords

Virtual Synchronous Machine (VISMA), power plant control, hysteresis controller, grid feed-in inverter, grid forming inverter

1. Introduction

The increasing use of renewable energy resources is driven on the one hand by the limited resources of fossil energy sources and on the other hand by energy policy objectives. This is also accompanied by a structural change in the energy grid from a centralised system to a decentralised system. System ancillary services, which were previously provided exclusively by large power plants, must now also be provided at lower grid levels [1]. The increasing expansion of renewable energy generation units in lower grid levels also has the effect that the power flow is reversed and energy flows from the lower to the upper grid levels.

The fundamental idea behind the Virtual Synchronous Machine (VISMA) concept is based on replicating the behaviour of an electromechanical synchronous machine by combining an inverter with an energy storage device and a digital signal processor (DSP hardware) [2]. The DSP calculates the electrical, magnetic and mechanical machine variables in real time using a mathematical model of the synchronous machine. The basic structure of such a system is shown in Figure 1. A complete VISMA system consists of a DC link to which an energy storage device (usually a battery) and optionally one or more DC generators are connected, a self-commutated IGBT power module with a LC output filter, a process computer for calculating the set values based on the actual values of the grid, and a current controller, in this case a hysteresis current controller.

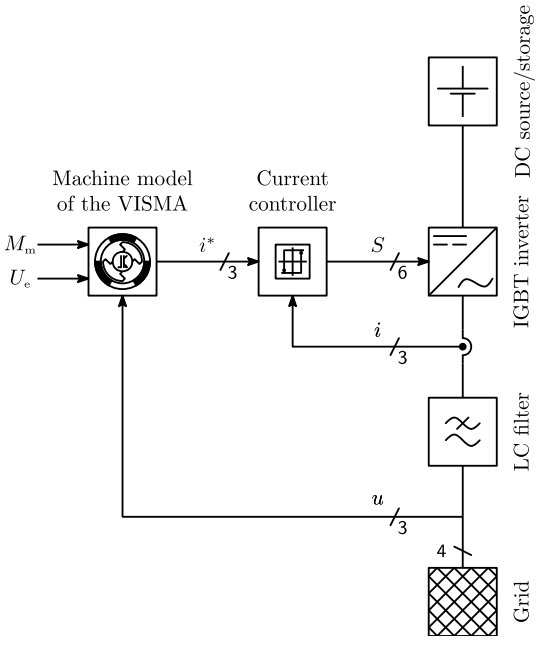

Fig. 1. Block diagram of the VISMA

Using the mathematical machine model according to equations (1) to (6), the DSP hardware calculates the phase currents from the voltage values at the grid connection point, which would set under the given conditions in a real synchronous machine. The determined phase currents are transferred to the phase current controller (hysteresis controller) and fed into the grid via the inverter.

For these investigations, the simplified machine model of the VISMA described by equations (1) to (6) is used [3].
The model is divided into three single-phase electrically effective stator circuits, each consisting of a voltage source u_e, which represents the virtual excitation voltage, a stator inductance L_s and the winding resistance R_s. The line voltage u_n is applied to the terminals of the equivalent circuit diagram. The resulting machine current is denoted by i. The mechanical subsystem of the machine is described from the equation of motion of the acting moments and its acting flywheel mass. The electrical subsystem is shown in Figure 2 and the mechanical subsystem is shown in Figure 3.

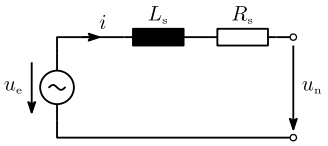

Fig. 2. The electrical equivalent circuit diagram of the VISMA

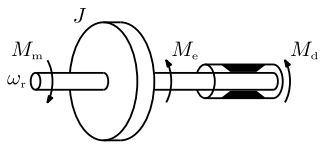

Fig. 3. The mechanical equivalent circuit diagram of the VISMA

The following system of differential equations can be derived from the equivalent circuit diagram of the electrical subsystem (cf. Figure 2):

$$\begin{bmatrix} u_{e,a} \\ u_{e,b} \\ u_{e,c} \end{bmatrix} = R_s \begin{bmatrix} i_a \\ i_b \\ i_c \end{bmatrix} + L_s \cdot \frac{d}{dt} \begin{bmatrix} i_a \\ i_b \\ i_c \end{bmatrix} + \begin{bmatrix} u_{n,a} \\ u_{n,b} \\ u_{n,c} \end{bmatrix} \quad (1)$$

The excitation voltages form a symmetrical three-phase voltage system with a phase shift of 120°, the amplitude $\hat{U}_e = \sqrt{2}\, U_e$ and the pole wheel angle θ_r.

$$\begin{bmatrix} u_{e,a} \\ u_{e,b} \\ u_{e,c} \end{bmatrix} = \hat{U}_e \begin{bmatrix} \sin(\theta_r t) \\ \sin(\theta_r t - \frac{2}{3}\pi) \\ \sin(\theta_r t + \frac{2}{3}\pi) \end{bmatrix} \quad (2)$$

The virtual excitation voltage U_e corresponds to the excitation voltage of a real machine and can be directly specified as an operating parameter in order to set the operating point of the machine.

The pole wheel angle θ_r is calculated from the integration of the virtual rotor angular frequency ω_r and thus couples the mechanical with the electrical subsystem.

$$\theta_r = \int \omega_r \, dt + \theta_r(t = 0) \quad (3)$$

The mechanical subsystem follows from the equivalent circuit of the rotor mechanics (see Fig. 3) via the corresponding equation of motion.

$$J \frac{d\omega_r}{dt} = M_m - M_e - M_d \quad (4)$$

Here, J is the mass moment of inertia of the virtual flywheel of the rotor and M_m describes the virtual mechanical torque on the shaft of the rotor. M_e describes the electrical torque via which the stator and rotor are coupled to each other and thus establishes the connection between the electrical and the mechanical submodel, and M_d describes the damping torque. The mechanical torque represents the second variable with which the operating point of the machine can be controlled from the outside.
The electrical torque acting on the rotor via the air gap of the machine is calculated by the instantaneous power of the stator circuit and the virtual rotor frequency. The stator power corresponds to the electrical power absorbed or delivered by the machine from the grid, depending on its operating point.

$$M_e = \frac{p_s}{\omega_r} = \frac{u_{e,a}\, i_a + u_{e,b}\, i_b + u_{e,c}\, i_c}{\omega_r} \quad (5)$$

To avoid pole wheel oscillations, a damping moment M_d is formulated in the form of a DT1-element. In other implementations of virtual flywheel masses, the grid frequency is included in the damping term. The model based on [3] does not receive the grid frequency as an input variable, the damping term was reformulated in such a way that it is dependent on its own change in speed. Therefore, no phase-locked loop (PLL) is required for the realisation of the VISMA.

$$M_d = K_d \cdot \frac{d\omega_r}{dt} - T_d \cdot \frac{dM_d}{dt} \quad (6)$$

The damping factor K_d and the filter time constant T_d are freely selectable, constant machine parameters, as are the stator inductance L_s, the winding resistance R_s and the mass inertia of the rotor J.

2. Control strategy

The manipulable variables of the VISMA are the virtual mechanical torque M_m on the shaft for the active power and the virtual excitation voltage U_e for the reactive power. The manipulated variables are independent of the operating mode of the VISMA – grid-parallel or island grid operation. For the investigations shown here, the virtual synchronous machine has a cascaded control consisting of a power plant control in the form of a P-controller with a downstream power control.

The primary controller is designed as a P-controller and receives the frequency deviation between the nominal grid frequency and the rotor frequency of the VISMA, which corresponds to the grid frequency, as an input variable. Depending on the set gain, the controller outputs a target active power to be fed in by the VISMA. Following [4], the controller has a dead band, also called insensitivity threshold, of ± 10 mHz, in which no regulation is active. The control is only activated at a frequency lower than 49,99 Hz or higher than 50,01 Hz. The entire control range of the primary controller is in a control band of 49,8 Hz to 50,02 Hz. The primary control power to be provided increases linearly from the minimum to the maximum frequency deviation. In the experiment presented in this paper, the controller sets the output power to 10 kW at the maximum frequency deviation of 200 mHz.

The secondary controller, the cascaded power controller, receives the power difference from the externally specified target active power P^* (in the experiments shown here, this value is zero), the target active power of the primary control P_{pc} and the actual active power that the inverter is feeding in at this instant. The power controller then tracks the virtual mechanical torque accordingly. The controller structure used here is similar to the controllers in power plants described in, for example, [5] and [6].

The basic structure of a VISMA system from Figure 1 is complemented by the corresponding control system, according to Figure 4.

The VISMA system consists of a 2-level B6 inverter with a downstream LC filter to suppress high-frequency components. A battery is connected on the DC side, which enables a bidirectional power flow. A two-point controller (hysteresis controller) is used as the current controller, which can directly regulate the setpoint current of the machine model in abc coordinates. Thus, a coordinate transformation and the use of a phase-locked loop is avoided.

3. Trial grid setup

For this paper, an experimental grid is set up according to Figure 5. It consists of two VISMA systems (both systems are parameterised identically), a load and a grid simulator to simulate the wide area synchronous grid. During the test, the coupling switch K1 is opened and the grid simulator is disconnected from the test grid. Thus, the investigated grid is transferred from grid parallel operation to island grid operation. According to [6] and [7], this setup corresponds to a typical microgrid.

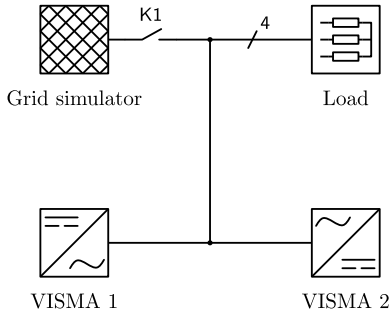

Fig. 5. Investigated experimental grid in the laboratory

4. Results

Figure 6 shows the resulting grid variables of the microgrid in Figure 5. At the time 5 s, the coupling contactor K1 is opened, thus disconnecting the test grid from the grid simulator and transferring it to an island grid. At the moment of opening the coupling contactor, the line voltage (top diagram in Figure 6) collapses briefly over a period of approx. 5 ms. Immediately after this voltage drop, the voltage takes on a sinusoidal course again, but with a reduced amplitude and a different frequency. The grid frequency now corresponds to the virtual rotor frequency of the VISMA.

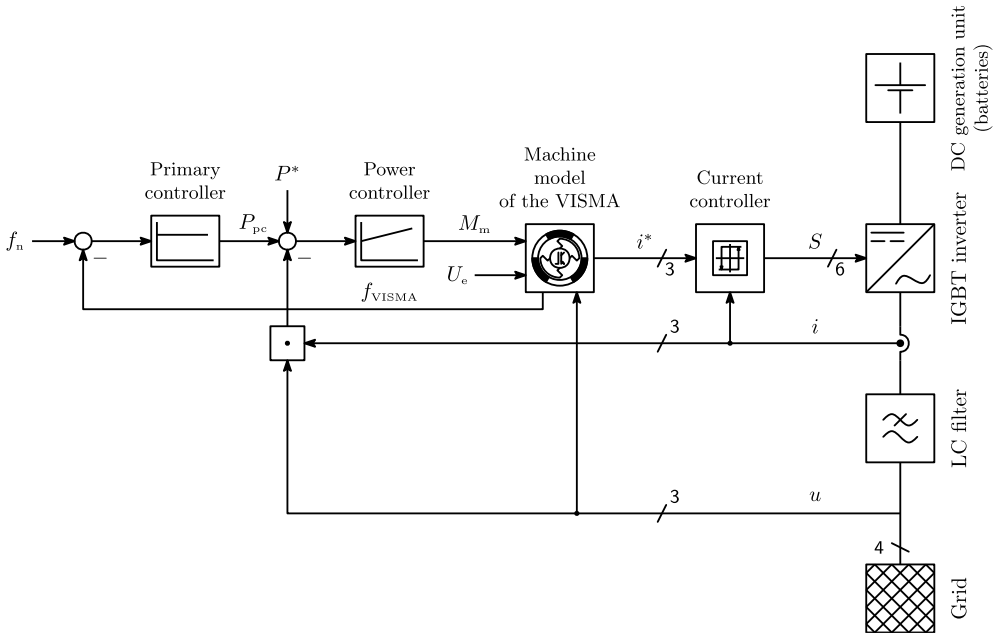

Fig. 4. Block diagram of the VISMA with the cascaded primary and power controller

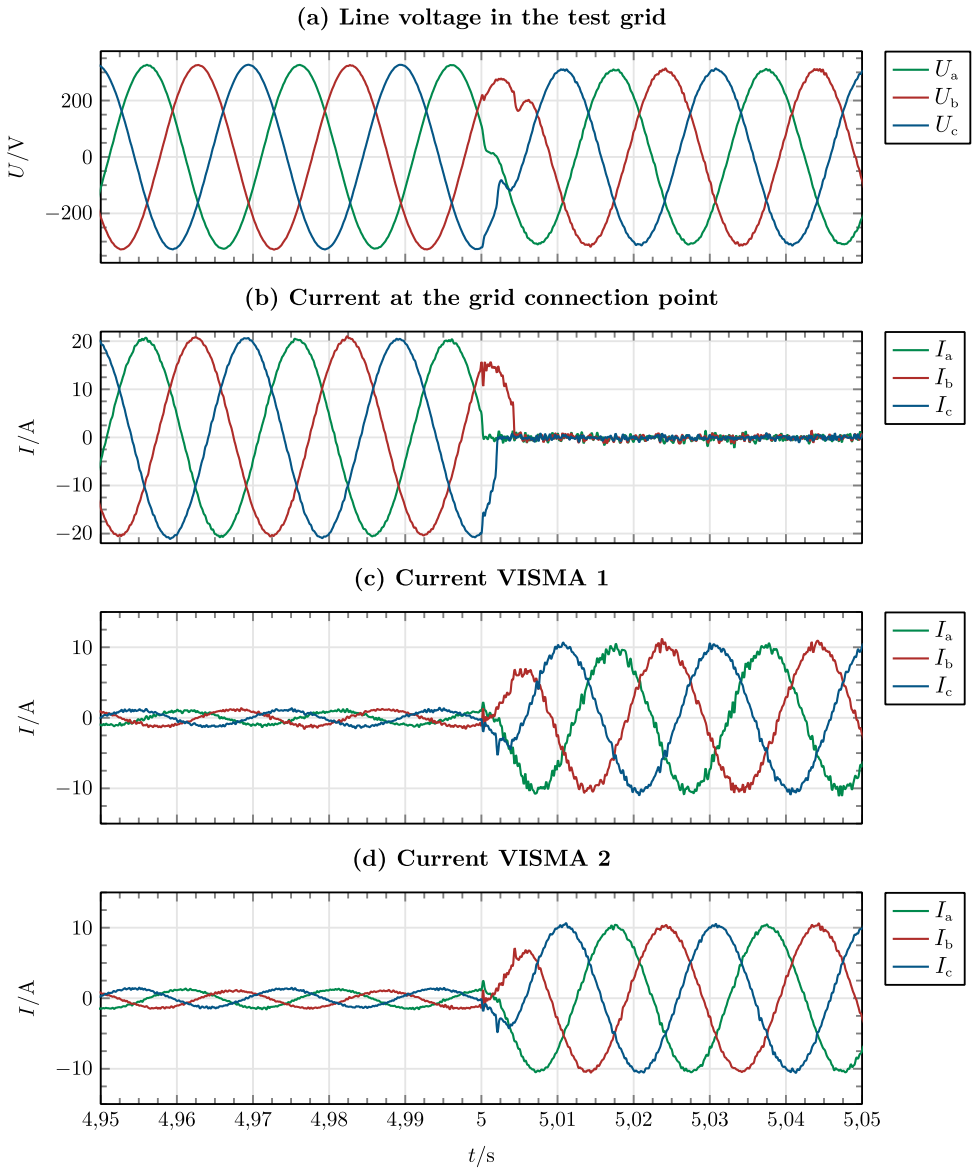

Fig. 6. Measurement results – grid failure in the decentralised distribution grid with VISMA. Transfer of the test grid with two VISMA systems from an interconnected grid to an island grid. The coupling contactor K1 (see Figure 5) opens at time 5 s. The VISMA systems are neutral in terms of active power until the grid is disconnected; the measured current before disconnection corresponds to the capacitive base load of the filter capacity of the inverter. The stabilisation of the island grid by the VISMA is completed 5 ms after the grid failure at time 5,005 s.

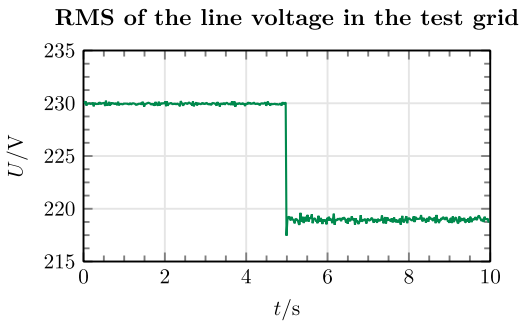

Fig. 7. Root mean squared (RMS) value of the line voltage in the test grid. Before the grid is disconnected, the voltage is 230 V and the voltage is specified by the grid simulator. After opening the mains contactor, the voltage drops below 220 V. A return to the nominal value is not possible due to the non-existing voltage control.

Figure 7 shows the effective line voltage during the test. The curve also clearly shows the voltage drop at the time of opening the coupling contactor. In grid-connected operation, the voltage is specified by the grid simulator and fixed to a value of 230 V. Due to the grid disconnection, the effective value of the voltage drops to below 220 V and the effective line voltage constantly deviates from its nominal value after the grid disconnection. This is because the VISMA in the test grid has no voltage control (see block diagram in Figure 4) and therefore the machine's excitation voltage, which can be used to influence the grid voltage, is not controlled.

Further investigations have shown that the grid voltage in the island grid after disconnection from the grid simulator depends on the load. The deviation from the nominal value can therefore also be significantly larger or smaller than shown here.

In addition to the grid voltage, Figure 6 (b) also shows the current at the grid connection point, which is the current supplied to the test grid by the grid simulator, and the currents of the two VISMA systems (Figure 6 (c) and (d)). The currents of the two VISMA systems are not zero before the grid disconnection. However, these are not active currents, but reactive currents of the capacitive base load (filter capacity at the inverter output) of the VISMA systems, which are located between the main contactor of the inverter and the measuring point. Active power is not fed in before the grid is disconnected, as the grid frequency is close enough to the nominal frequency of 50 Hz (see Figure 8 and 9). The fact that the VISMA does not feed in any active power at this point is also due to the primary control (frequency-dependent active power setpoint), which specifies zero as the setpoint (see Figure 10), since the grid frequency corresponds to the nominal value.
The transient of the fed-in current of the two VISMA systems is approximately 5 ms, i.e. exactly the duration of the voltage dip. After this short time, the transient process is already completed and the two VISMA systems have completely taken over the supply of the load. This behaviour can also be seen in Figure 8. At 5 s, the power feeding into the test grid via the grid connection point (gcp) turns zero due to the disconnection (opening of the grid contactor K1, cf. Figure 5) and the two VISMA systems feed into the test grid according to their primary control characteristic and thus completely supply the load. The reduced power consumption of the ohmic load resistor in the island grid can be attributed to the fact that the grid voltage is lower than before the disconnection.

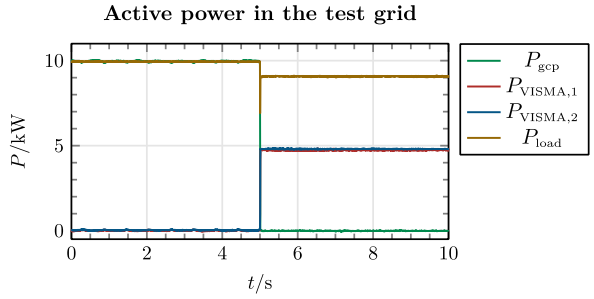

Fig. 8. Active power feed-in into the test grid via the grid connection point (feed-in power of the grid simulator) P_{gcp} and of the VISMA systems $P_{VISMA,i}$ as well as the consumer power of the ohmic load resistor P_{load}. Before the grid disconnection at 5 s, the load is completely supplied by the grid simulator. The VISMA systems do not feed in any power at this time. After disconnection, the two VISMA systems take over the supply of the load. The load is distributed equally to both systems due to the same parameterisation.

The drop in the virtual rotor frequency can be seen in Figure 9. The upper diagram shows the variation of the rotor frequency in a range from 5 s before to 5 s after the transfer of the test grid from grid-parallel operation to island grid operation. The frequency fluctuations of less than 10 mHz before grid disconnection are due to the grid voltage of the grid simulator. However, because the primary control has a dead band of ± 10 mHz, the VISMA systems not react at this point.

The transition to the new steady state of the island grid takes about 40 ms, cf. Figure 9. After this time, the rotor frequency of the VISMA stabilises and remains constant at 49,91 Hz starting at 5,04 s. The rotor frequency is used as an input variable for the primary control and the required control power is calculated and transferred to the VISMA as a setpoint (compare Figure 10).

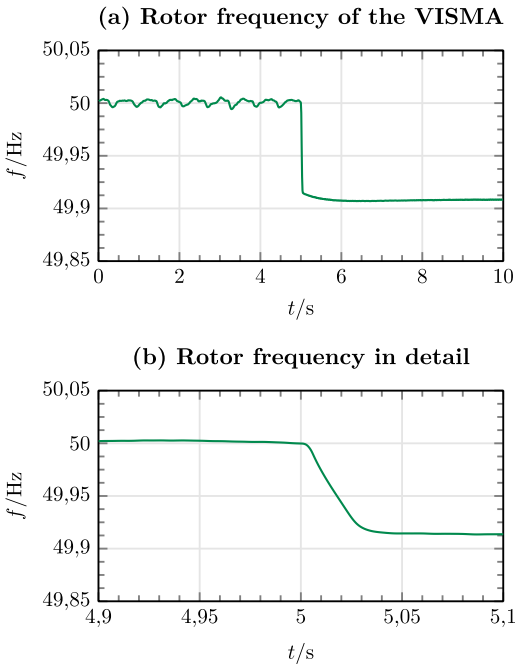

Fig. 9. Frequency of the virtual flywheel of the VISMA, which at the same time corresponds to the grid frequency of the experimental grid. Before grid disconnection, the grid frequency is specified by the grid simulator. With the transition to island operation, the frequency drops. The drop ensures that the primary controller is activated and outputs a target active power. The grid frequency stabilises when an equilibrium is reached between generated and consumed active power in the test grid. This occurs after 40 ms.

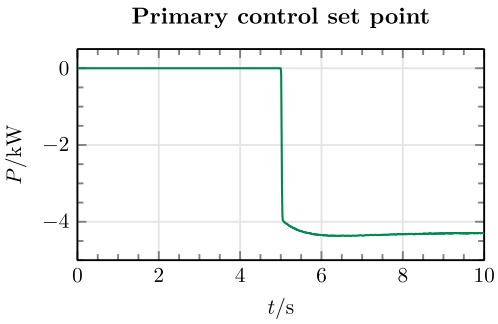

Fig. 10. Calculated active power of the primary power controller as a function of the grid frequency in Figure 9.

5. Conclusion

The results presented in this paper show that the virtual synchronous machine is able to provide grid parallel operation and island operation with uninterrupted transition between the operation modes with one and the same controller. The primary controller is able to participate in the ancillary services in grid-parallel operation and makes

stable grid operation possible in the island grid. This has the advantage that communication between several VISMA systems can be dispensed with and the grid structure is very modular.

The experiment shown here only has a controller for frequency maintenance, the voltage regulation was not discussed here. However, further experiments have already shown that a comparable controller for voltage control already works in pure island grid operation. Experiments are still pending for both grid operation.

Acknowledgments

We gratefully acknowledge support from the Federal Ministry of Education and Research (BMBF grant no. 03EK3055G).

References

[1] B. Werther, Stabilitätsanalyse zur Bereitstellung von Momentanreserve am frequenz-starren Übertragungsnetz durch einen mittelspannungsnetzseitigen Verbund virtueller Synchronmaschinen, 1. Auflage. Göttingen: Cuvillier Verlag, 2022.

[2] H.-P. Beck and R. Hesse, 'Virtual synchronous machine', in 2007 9th International Conference on Electrical Power Quality and Utilisation, Barcelona, Spain: IEEE, Oct. 2007, pp. 1–6.

[3] Y. Chen, Virtuelle Synchronmaschine (VISMA) zur Erbringung von Systemdienstleistungen in verschiedenen Netzbetriebsarten, 1. Auflage. in Schriftenreihe des Energie-Forschungszentrums Niedersachsen (EFZN), no. Band 41. Göttingen: Cuvillier Verlag, 2016.

[4] VDE FNN, 'VDE-AR-N 4120: Technische Regeln für den Anschluss von Kundenanlagen an das Hochspannungsnetz und deren Betrieb (TAR Hochspannung)'. VDE-Verlag, Berlin, Nov. 2018.

[5] K. Heuck, K.-D. Dettmann, and D. Schulz, Elektrische Energieversorgung. Wiesbaden: Springer Fachmedien Wiesbaden, 2013. doi: 10.1007/978-3-8348-2174-4.

[6] A. J. Schwab, Elektroenergiesysteme: Smarte Stromversorgung im Zeitalter der Energiewende. Berlin, Heidelberg: Springer Berlin Heidelberg, 2020. doi: 10.1007/978-3-662-60374-1.

[7] V. Crastan and D. Westermann, Elektrische Energieversorgung 3: Dynamik, Regelung und Stabilität, Versorgungsqualität, Netzplanung, Betriebsplanung und -führung, Leit- und Informationstechnik, FACTS, HGÜ. Berlin, Heidelberg: Springer Berlin Heidelberg, 2018. doi: 10.1007/978-3-662-49021-1.